Seafloor Ground Rotation Observations: Potential for Improving Signal-to-Noise Ratio on Horizontal OBS Components

by Fabian Lindner, Joachim Wassermann, Mechita C. Schmidt-Aursch, Karl Ulrich Schreiber, and Heiner Igel

ABSTRACT

We report the first ground rotation observations on the seafloor from an experiment we carried out in the North Sea close to the island of Heligoland. A slightly modified commercial fiber optic gyroscope was mounted on an ocean-bottom seismometer (OBS) platform together with an intermediate-period seismometer. The system was lowered to the seafloor for 4 days. To investigate a potential tilt contamination of horizontal translational recordings, we calculate the coherence between the corresponding motion components (rotations around x axis and translations along y axis, and vice versa). We find very high correlations in the 5–13 s period interval, in which the correlation coefficient reaches 0.94 over 8.5 hrs. This clearly indicates that horizontal translational components are severely contaminated by rotations. We find that these rotational motions are caused by seafloor currents or deformation of the seafloor rather than by seismic waves. The ground rotation observations allow correcting for the cross-coupling effect, thereby decreasing the power spectral density up to 11 dB at 10 s period on horizontal OBS components. We discuss general requirements for broadband rotation sensors for OBS applications as well as for possible further applications.

INTRODUCTION

Since the advent of ocean-bottom seismometers (OBS), data can also be gathered in offshore areas. The first long-period instrument was deployed in 1965 and subsequently led to the availability of broadband seismic data at the ocean floor (Sutton *et al.*, 1965). However, observations revealed that horizontal components suffer from poor data quality when compared with vertical components (e.g., Webb, 1988; Duennebier and Sutton, 1995). Duennebier and Sutton (1995) conclude that this might be the reason that early studies focused on vertical-component data. More recent studies also report this significant difference in data quality between the horizontal and vertical components (e.g., Crawford and Webb, 2000; Dahm *et al.*, 2006; Pillet *et al.*, 2009; Yang *et al.*, 2012). This especially holds for long-period records of periods longer than 10 s in which the difference in noise level may exceed as much as 45 dB (Crawford and Webb, 2000). The reason for this observation is assumed to be caused by tilting: when rotated from the horizontal plane, seismometers become sensitive to the Earth's gravitational acceleration and record a signal that they are not intended to measure. Seismic data can thus be contaminated by rotational motions, especially affecting horizontal components (Rodgers, 1968; Graizer, 2006). In marine environments, long-period tilting of OBS systems is thought to originate from the interaction of water currents, the OBS exterior, and the seafloor boundary layer (e.g., Webb, 1988, 1998; Crawford and Webb, 2000).

To correct for or even avoid tilt contamination, different approaches have been introduced. Crawford and Webb (2000) exploit coherence on horizontal and vertical components caused by tilting to remove the contamination from the latter. In contrast to that, Collins *et al.* (2001) and Araki *et al.* (2004) try to improve the installation environment of the instruments. To reduce horizontal long-period noise caused by the interaction of water flow, boundary layer, and instrument housing, they bury the OBSs and deploy them in boreholes. However, in general, direct observation, quantification, and correction of horizontal tilt effects have not been reported so far.

Ring laser gyroscopes that measure the vertical component of rotation rate proved successful for recording seismically induced rotational ground motions due to earthquakes (McLeod *et al.*, 1998; Pancha *et al.*, 2000; Igel *et al.*, 2005) and ambient noise (Hadziioannou *et al.*, 2012). Nevertheless, portable rotation sensors (and thus instruments capable of measuring the tilting of OBS systems) have previously not been found suitable for weak motion seismology because they lack sensitivity (Bernauer *et al.*, 2012).

In this study, we present a novel instrumentation setup consisting of a three-component rotational sensor rigidly attached to an OBS system. Our basic approach is to use this six-degree-of-freedom (6-DOF) measurement to quantify the tilt contamination of horizontal OBS components. In the following sections, we describe the experiment, data analysis, and our results.

 doi: 10.1785/0220160051

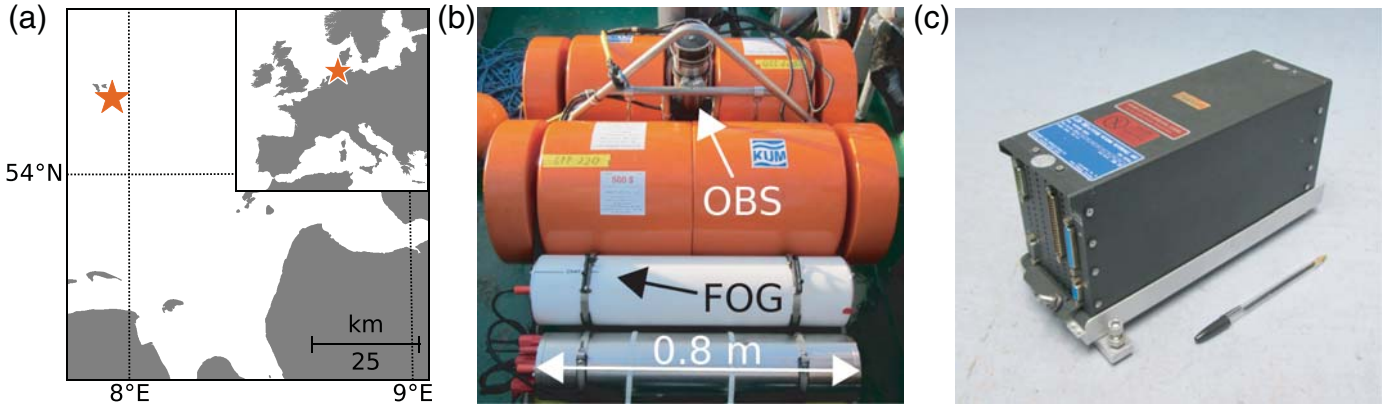

▲ **Figure 1.** (a) Deployment site of the sensor system. The orange star indicates the deployment location of the sensor system close to the island of Heligoland in the North Sea. (b) The sensor system consisting of the intermediate-period ocean-bottom seismometer (OBS) Güralp CMG-OBS40T and the rotational sensor Northrop Grumman LITEF LCG-Demonstrator. The OBS system is completed by an analog hydrophone. (c) The Northrop Grumman LITEF LCG-Demonstrator. The fiber optic gyroscope (FOG) measures three components of rotation rate and translational acceleration.

EXPERIMENT

We report on direct observations from a novel instrumentation setup dedicated to measuring dynamic tilting of OBS systems for, to our knowledge, the first time. In May 2014, we deployed the three-component rotation sensor Northrop Grumman LITEF LCG-Demonstrator collocated with an intermediate-period seismometer (Güralp CMG-OBS40T) at the ocean bottom. In principle, the LCG-Demonstrator works as a fiber optic gyroscope (FOG), exploiting the Sagnac effect (e.g., Schreiber *et al.*, 2009; Bernauer *et al.*, 2012). In this massless measurement system, two laser beams associated with wavelength λ counter propagate in a loop that encloses an area A. If the apparatus rotates with angular velocity $\dot{\Omega}$, the two laser beams exhibit a phase difference given by

$$\delta\phi = \frac{8\pi NA}{\lambda c}\mathbf{n}\cdot\dot{\Omega}, \tag{1}$$

in which N is the number of turns of fiber, $\mathbf{n}$ is the normal vector upon A, and c is the speed of light. The dot product $(\mathbf{n}\cdot\dot{\Omega})$ gives the orientation of the sensor with respect to the vector of rotation. Besides the measurement of rotation rate, the LCG-Demonstrator also records three components of translational acceleration. Both quantities are sampled at 200 Hz. Because the measurement principle is purely optical and no masses are involved, the frequency response of the FOG is constant through the entire spectrum. The resolution limit is determined by the sensor's self-noise of 2×10^{-7} rad/s at 10 s period. Although the self-noise is decreasing at longer periods, the least significant bit (LSB) value of 2×10^{-7} rad/s prevents measuring smaller rotation rate amplitudes in the current setup. For details on the FOG, the reader is referred to Bernauer *et al.* (2012). The seismometer is characterized by a corner period of 60 s and is equipped with a gimbal-leveling system that was activated 10 hrs after deployment. However, the vertical component was not released properly and did not record useful data. In addition to the motion sensors, a hydrophone was mounted to the platform, measuring differential pressure. As for the seismometer, it also has a flat response down to 60 s and was digitized by the same data logger. For details on the seismometer and the hydrophone, the reader is referred to Stähler *et al.* (2016).

The seismometer and rotation sensor are rigidly attached to the OBS frame, and the latter is mounted horizontally by means of visual judgment. We are confident that the frame acts as a perfectly rigid body such that the seismometer and FOG experience the same motions. To ensure that all instruments acquire data synchronously, both recorders were synchronized via Global Navigation Satellite Systems services prior to the deployment. For this purpose, the FOG is linked to a Meinberg GPS180XHS type Global Positioning System that provides a time stamp with better accuracy (i.e., it has a smaller drift) than the clock of the OBS recorder. The management of rotation data acquisition and storage is accomplished by a Raspberry Pi computer.

The whole system was lowered to the seafloor in the North Sea close to the island of Heligoland (see Fig. 1) at a depth of 30 m. The water temperature for this shallow deployment is not expected to be as stable as for deep-ocean deployments. Nevertheless, the temperature within the data logger housing did not show variations greater than 1°, which should not affect the measurements (see Bernauer *et al.*, 2012). Because FOGs are commonly used for navigation purposes, the field installation implied some limitations for the experiment. First, waterproof housing for the additional instruments of this prototype sensor system in a plastic tube restricted the deployment to shallow water. Second, the power consumption of the LCG-Demonstrator of 28 W (plus some Watts for clock and computer) is much higher than that of the OBS system (0.72 W at 1000-Hz sampling rate). This constrained the duration of the deployment to only about 4 days using lithium battery packs.

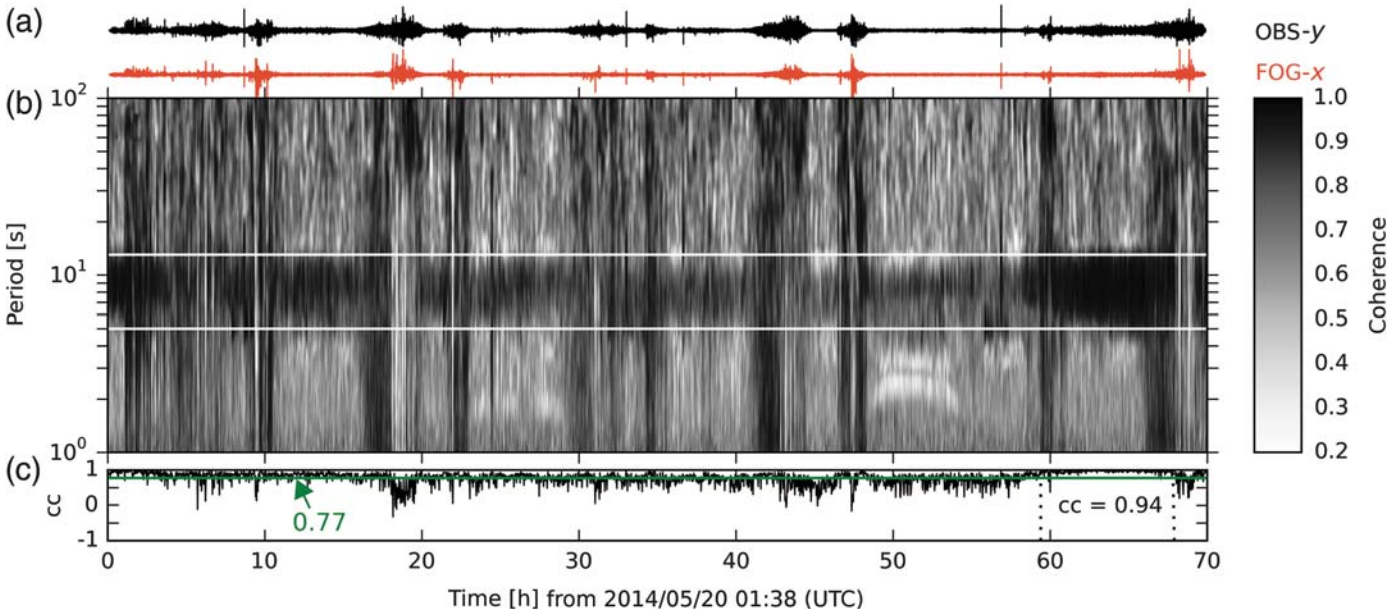

▲ **Figure 2.** (a) Acceleration along the *y* axis obtained from the seismometer (black) and rotation around the *x* axis multiplied by the Earth's gravitational acceleration (red). (b) Coherence between these two data sets as a function of time and period. The two horizontal white lines indicate the period band from 5 to 13 s in which high coherence is observed. (c) Correlation coefficient (cc) of the waveforms in this period band. The green line indicates the average value of 0.77. Toward the end of the time series, the correlation coefficient reaches an average value of 0.94 in an 8.5-hr time interval. Note that this is associated with increased amplitudes of translational and tilt acceleration.

The deployment location was chosen close to a natural reserve to ensure that data acquisition was not disturbed by fishing activities. The seafloor surface in the area next to the deployment is characterized by coarse sand and crushed shells (BSH Seekarte Nr. 88, Helgoland, Maßstab 1:12,500).

DATA ANALYSIS

Tilt sensitivity of seismometers is discussed in detail by Graizer (2006, 2009). Accordingly, the response x of the horizontal x-component of a seismometer is described by

$$\ddot{x} + 2\omega_x D_x \dot{x} + \omega_x^2 x = -\ddot{u}_x + g\Omega_y, \tag{2}$$

in which y denotes the horizontal y-component, ω_x and D_x are the natural frequency and fraction of critical damping of the x-oscillator, respectively, and g is the Earth's gravitational acceleration. Following equation (2), the x-oscillator is sensitive to the translational acceleration $\ddot{u}_x$ along the x axis and to tilting Ω_y around the y axis, respectively, and vice versa for the y-oscillator. This formulation does not include the displacement effect of tilting, which is proportional to the distance of the sensor to the center of mass of the whole platform. Crawford and Webb (2000) show that this effect should only be important for higher frequencies (>1 Hz), which is why we do not consider it in our data set. In addition, the terms for cross-axis sensitivity and angular acceleration are not considered as they can be neglected for small oscillations (e.g., Graizer, 2009).

Equation (2) tells us that horizontal recordings of a seismometer are a superposition of linear acceleration and angular displacement (multiplied by g). Because all recordings in our measurement setup are obtained in velocity, data are processed as follows. First, we correct the OBS data for instrument response and differentiate it with respect to time, to obtain acceleration. Recordings from the FOG have been divided by a frequency-independent gain factor and are afterward integrated with respect to time, resulting in rotations in terms of angles. Finally, these rotations are multiplied by the Earth's gravitational acceleration. All processing is done with the ObsPy toolbox (Beyreuther *et al.*, 2010; Megies *et al.*, 2011). In this article, we call the couple y-translation–x-rotation motion pair 1 (MP1) and the couple x-translation–y-rotation motion pair 2 (MP2).

In the frequency band around 10 s period, Figure 2 indicates that tilt acceleration caused by rotation around the x axis is coherent with the translational acceleration along the y axis (MP1). This especially holds toward the end of the time series in which the coherent period band even broadens. Coherence generally seems to increase with increasing amplitudes. Transient broadband coherence features ranging from 1 to 100 s are associated with strong signals. For the second pair of corresponding motion (MP2), coherence is generally low (not shown). Nevertheless, from around 61.5 to 68 hrs of the time series, MP2 is also highly coherent. In the following, unless MP2 is explicitly mentioned, the focus is on MP1.

We isolate the highly coherent period band from 5 to 13 s by applying a Butterworth zero-phase band-pass filter to both

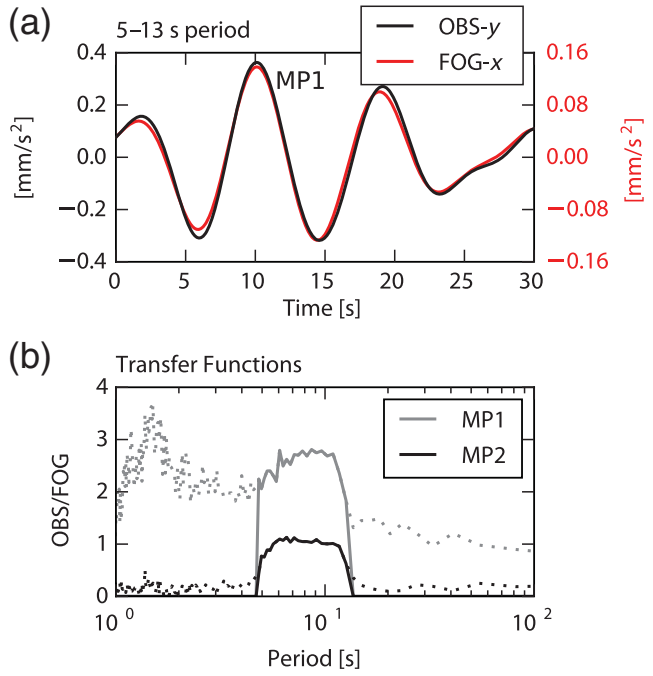

▲ **Figure 3.** (a) Sample waveforms of translational acceleration and tilt acceleration of MP1 (translational along *y* axis, rotation around *x* axis). Note that amplitudes of the latter are generally smaller. (b) Magnitude of transfer functions between tilt acceleration and translational acceleration. Solid lines indicate the band-limited version of the transfer function used to remove the tilt noise from the horizontal OBS recordings. Outside of this frequency range (dotted lines), no tilt noise removal is performed because coherence is generally low.

time series. To quantify the similarity between the waveforms, the correlation coefficient is calculated in a sliding window of 100 s length. Figure 2 shows that the correlation coefficient averages 0.77 over 70 hrs, indicating that tilt acceleration and translational acceleration are strongly correlated. In an 8.5-hr window toward the end of the experiment, the correlation coefficient reaches on average 0.94, meaning that the waveforms are almost identical (Fig. 3). This part coincides with increased amplitudes of the recorded signals. Nevertheless, strong signals at 19, 47, and 68 hrs of the time series cause a decrease in the coherence and correlation coefficient. During these times, the horizontal component sticked to the clipping level for several seconds before changing the polarity and sticking again to the (opposite) clipping level. The source of these signals is not known but is likely due to strong OBS movement rather than caused by instrument malfunction. The MP2 correlation coefficient averages 0.49 and reaches 0.91 in a 6.5-hr subinterval of the high-correlation MP1 interval.

In the considered period range, the tilt-induced acceleration contaminating the translational data reaches $10^{-5} - 10^{-4}$ m/s^2 in amplitude. This translates to $10^{-6} - 10^{-5}$ rad and rad/s in terms of rotation and rotation rate, respectively. Because we directly quantify these rotations, the FOG data can be used to remove the tilt noise from the horizontal OBS components. For this purpose, we calculate the frequency-dependent transfer function between the tilt acceleration and the translational acceleration. Crawford and Webb (2000) introduce it as

$$A_{rs}(f) = \gamma_{rs}(f)\sqrt{\frac{G_{rr}(f)}{G_{ss}(f)}}, \tag{3}$$

in which G_{rr} and G_{ss} denote the one-sided autospectral density functions of the response channel r (translational acceleration) and source channel s (tilt acceleration), respectively. The square root of their ratio is tapered by the coherence function γ_{rs} between the two channels. In the frequency domain, the tilt corrected seismometer signal R' is then calculated by

$$R'(f) = R(f) - A^*_{rs}(f)S(f), \tag{4}$$

in which R and S are the fast Fourier transforms of the translational and tilt acceleration, respectively, and the asterisk denotes complex conjugation.

We calculate the transfer function from windowed sections of the 8.5-hr data interval of strong correlation. Subsequently, we apply equation (4) to the windowed data to remove the tilt noise. The same is done for MP2 in the 6.5-hr high-correlation interval. Figure 3 shows the transfer functions for a broad frequency range, but we use only the high-coherence interval from 5 to 13 s period to remove the tilt noise. The result is shown in Figure 4, which reveals that the *y*-component power spectral density (PSD) is decreased by 11 dB at 10 s period and the *x*-component PSD by 9 dB after tilt removal. The power spectra are associated with a strong peak in the considered period range that does completely vanish for MP1 only. To evaluate the influence of the displacement effect of tilting, we also consider it in the transfer function. As expected, this term has no effect on the tilt removal in the considered period band.

Tilt acceleration amplitudes are generally smaller than those of the tilt contaminated seismograms. Additionally, *y*-translations are higher in amplitude than *x*-translations (Fig. 4), but rotation amplitudes are similar for both horizontal FOG components (not shown). This reveals that the ratio between translation and tilt acceleration amplitude is higher for MP1 (compared with MP2) that can also be seen from the transfer functions. Figure 3 shows that the translation amplitude exceeds the tilt amplitude by almost a factor of 3 for MP1, whereas they are approximately equal for MP2.

To investigate the origin of the peaks associated with tilting, we compared pressure data from the hydrophone and recordings from station HLG located in Heligoland with the OBS recordings (the distance from HLG–OBS is roughly 4 km). In the same time interval, the PSD of the hydrophone also peaks around 10 s and is generally similar in shape. In contrast, station HLG shows very different spectral characteristics (Fig. 4). To compare both seismic sensors, horizontal recordings of station HLG are rotated to align them to the OBS. Because the Earth's rotation rate is seen by the FOG as constant offsets of different amplitude on the three components, we can

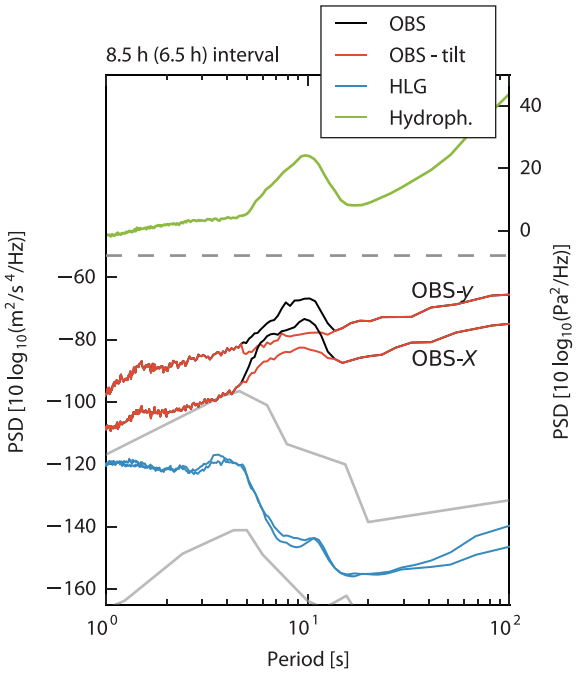

▲ **Figure 4.** Power spectral density (PSD) for the horizontal OBS components before and after tilt correction derived from MP1 (translation along *y* axis and rotation around *x* axis) and MP2 (translation along *x* axis and rotation around *y* axis). The frequency-dependent transfer function (see Crawford and Webb, 2000) is used to remove the tilt noise from the horizontal translational components. Also shown are PSDs of the horizontal components of station HLG (distance roughly 4 km to the OBS) and of pressure perturbations observed by the hydrophone at the OBS. The solid gray lines indicate the low-noise and high-noise model by Peterson (1993). Note that all PSDs are processed from 8.5 hrs of data, except for MP2, for which only 6.5 hrs are used.

estimate the true misalignment of the FOG versus geographic north. Power spectra of HLG horizontals are much lower than those of the OBS, especially for periods longer than 5 s. Furthermore, the HLG PSDs are associated with two distinct peaks at roughly 4 and 11 s. Further analysis did not show any coherence between hydrophone and the OBS or between station HLG and the OBS.

DISCUSSION AND CONCLUSION

We show that horizontal components of our OBS deployment are severely contaminated by rotational motions. By subtracting the tilt-induced acceleration, the noise level could be improved significantly in the period range from 5 to 13 s. Because the seismometer is self-leveling, the axes of OBS and FOG were not perfectly aligned. To quantify this effect, we estimate the misalignment between the axes. From the permanent offset of the FOGs' accelerometers, the platform tilt at the seafloor is determined to be less than 3°. Assuming that the error introduced by leveling the FOG by visual judgment is at most 5°, the maximum possible misalignment between OBS and FOG axes is less than 8°. The error introduced thereby can be quantified by rotating the FOG horizontally using Euler angle rotations. It shows that the amplitude is affected by at most 4.5% in our case. However, this value is reached only for the unlikely case that all three rotation rate components are in phase. Considering the amplitudes of the observed rotation rates in the 5–13-s period band, the error in amplitude caused by misalignment should be beyond the self-noise level of the FOG most of the time. For this reason, our results are considered resilient regarding the sensor installation setup.

To evaluate different mechanisms that might cause the tilting, we start with the assumption that a connection between wave heights and tilting exists. Because buoys close to Heligoland were not operational during the experiment, we rely on data from the WAVEWATCH III model (Tolman, 1997, 2009). During the experiment, the significant wave height reaches 3.5 m in the central North Sea. Because ocean waves can excite microseismic noise far from the receivers (Longuet-Higgins, 1950; Kedar *et al.*, 2008), we consider the significant wave height in the entire North Sea (see Fig. 5). For each timestep (wave heights are sampled every three hours), we integrate over the whole area and divide by the number of grid points to obtain one representative curve. Figure 5 shows that the average significant wave height correlates with the envelope of HLG data filtered between 5 and 13 s. In contrast to that, FOG and OBS data are correlated with pressure perturbations in the high-correlation interval toward the end of the experiment. A direct connection to wave heights as seen for station HLG cannot be discerned. In addition, the adjacent land-station HLG shows a significantly different power spectrum. A peak in the considered period band is not present, and the noise levels are much smaller compared with that of the OBS. These observations suggest that the OBS tilt noise is not caused by Rayleigh waves induced by microseisms that cause rotations around the horizontal axes.

More likely, the tilt signature is caused by the direct interaction of the ocean with the seafloor and the OBS. In a review of noise observed at the seafloor, Webb (1998) separates the long-period band from the short-period band by the microseismic peak centered at 5 s. Accordingly, long-period noise (longer than 10 s) on horizontals is most likely caused by seafloor currents, whereas the microseism is generated by seismic surface waves. However, in shallow water, different noise sources become dominant. Webb and Crawford (2010) show that for water depths as small as 50 m, the deformation of the seafloor due to loading of wind-driven waves is significant in the considered frequency band. This deformation is suitable to explain the presence of rotational noise since local tilting of the seafloor is involved. To confirm this theory, we however need to evaluate vertical-component translation data, which is not available due to instrument malfunction.

Another source of the rotational motions in the period band around 10 s could be the interaction of water motion with the OBS exterior. There is no coherence between the OBS and hydrophone data. Nevertheless, power spectra of both sensors are similar, and strong pressure perturbations are

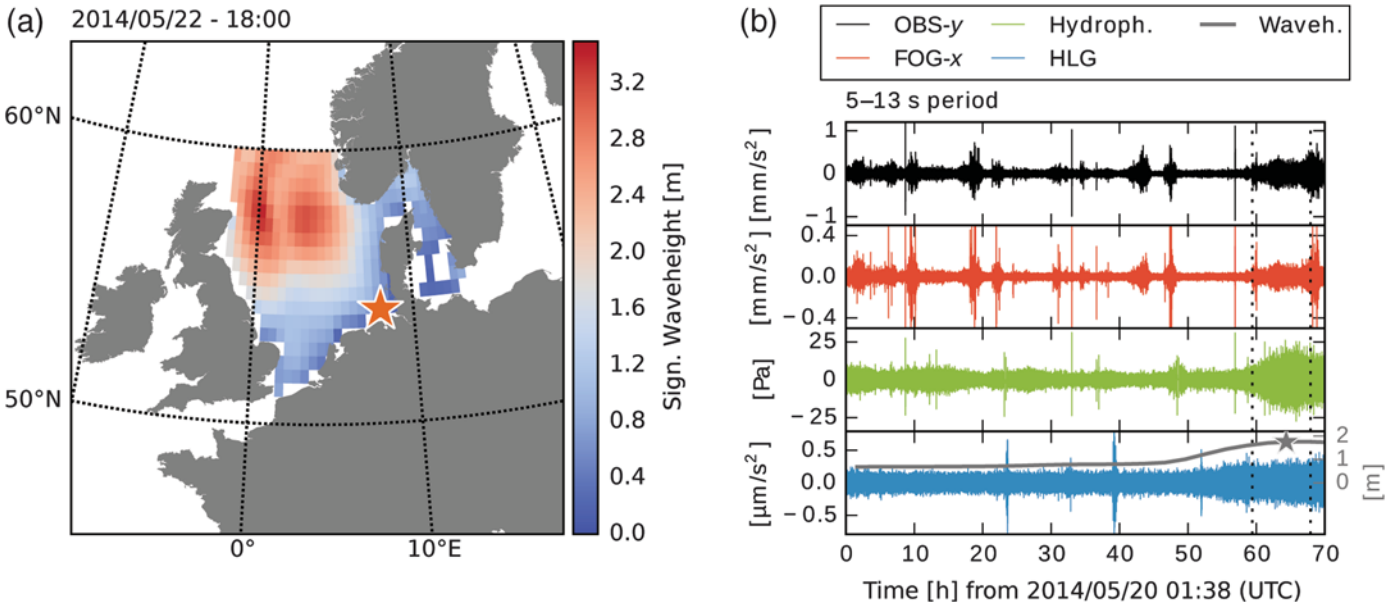

▲ **Figure 5.** (a) Significant wave height in the North Sea on 22 May 2014 at 18:00 obtained from the WAVEWATCH III model (Tolman, 1997, 2009). The orange star indicates the deployment location. (b) Translational acceleration (black), corresponding tilt acceleration (red) of MP1, and pressure perturbations (green) observed at the OBS system. The bottom trace shows translational acceleration observed at station HLG (parallel to top trace) and the average wave height in the North Sea (gray). The latter is obtained by the integral over the colored area in (a), divided by the number of grid points. The gray star corresponds to the situation illustrated in (a). Black dotted lines indicate the 8.5-hr time interval of strong correlation.

present at 10 s period. Furthermore, the increase in amplitude in the 8.5-hr interval of both recordings correlates well. A potential explanation is that water masses pushing and pulling the OBS system cause a displacement of the whole sensor system. This should be registered by the hydrophone as it is accelerated with respect to the water column. Because of insufficient stiffness of the sandy seafloor, the proposed mechanism should excite rotations besides translations. This potentially also explains why MP1 exhibits a strong translation component (OBS/FOG >1 and OBS-y $>$; OBS-x; see Figs. 3 and 4, respectively), which could originate from a dominant direction of water motion parallel to the seismometer's y axis.

Duennebier *et al.* (1981) also report that horizontal long-period tilt noise is caused by seafloor currents. However, Crawford and Webb (2000) discern this tilt noise for periods greater than 10 s only. The limit for longer periods in our case might be caused by the sensitivity of the FOG. For example, at 100 s period, rotation rates that correspond to tilt amplitudes of 1×10^{-6} rad are below the LSB value of 2×10^{-7} rad/s and cannot be resolved by the FOG. This is the case because the integration from rotation rate to rotation angle involves a multiplication with the period. Furthermore, a broadband seismometer would be necessary to investigate long-period effects.

The fact that noise levels are high in our case when compared with deep-sea experiments (compare with Crawford *et al.*, 2006) illustrates that portable rotation sensors are currently lacking in sensitivity. Besides improvements in sensitivity, these sensors must have a significantly lower power consumption to be useful for routine OBS applications. Apart from tilt removal from horizontal components, three-component rotation sensors can be used to determine the orientation of OBS systems at the seafloor using the Earth's rotation as a reference frame. In addition, collocated measurements of translation and rotation can be used to derive local phase velocity information (e.g., Igel *et al.*, 2005). These applications make them additionally attractive for marine seismology and highlight that further instrument development should be undertaken.

DATA AND RESOURCES

Seismograms used in this study were collected using a modified ocean-bottom seismometer system from the Deutscher Geräte-Pool für amphibische Seismologie/German instrument pool for amphibian seismology (DEPAS) Pool. Plots were made using Matplotlib (Hunter, 2007).

ACKNOWLEDGMENTS

We gratefully acknowledge support from the European Research Council (ERC)-Advanced project Rotational Motions in Seismology (ROMY) and thank the DEPAS Pool and Northrop Grumman LITEF GmbH for providing us with ocean-bottom seismometer (OBS) and rotation sensor, respectively. We are grateful to Sven Egdorf and Werner Bauer for their efforts in planning and setting up the sensor system. Many thanks also to Henning Kirk and Maria Tsekhmistrenko for their help on the deployment and recovery cruise, as well as to the whole crew of the research vessel Uthoern and to Philipp Fischer for organizing the cruises. We further thank Simon Stähler and Céline Hadziioannou for helpful discussions

and comments. We acknowledge the support and discussions within Time Dependent Seismology (TIDES) European Cooperation in Science and Technology (COST) Action ES1401 and would like to thank two anonymous reviewers for their valuable comments and suggestions.

REFERENCES

Araki, E., M. Shinohara, S. Sacks, A. Linde, T. Kanazawa, H. Shiobara, H. Mikada, and K. Suyehiro (2004). Improvement of seismic observation in the ocean by use of seafloor boreholes, *Bull. Seismol. Soc. Am.* **94,** no. 2, 678–690.

Bernauer, F., J. Wassermann, and H. Igel (2012). Rotational sensors—A comparison of different sensor types, *J. Seismol.* **16,** no. 4, 595–602.

Beyreuther, M., R. Barsch, L. Krischer, T. Megies, Y. Behr, and J. Wassermann (2010). ObsPy: A python toolbox for seismology, *Seismol. Res. Lett.* **81,** no. 3, 530–533.

Collins, J., F. Vernon, J. Orcutt, R. Stephen, K. Peal, F. Wooding, F. Spiess, and J. Hildebrand (2001). Broadband seismology in the oceans: Lessons from the ocean seismic network pilot experiment, *Geophys. Res. Lett.* **28,** no. 1, 49–52.

Crawford, W. C., and S. C. Webb (2000). Identifying and removing tilt noise from low-frequency (< 0.1 Hz) seafloor vertical seismic data, *Bull. Seismol. Soc. Am.* **90,** no. 4, 952–963.

Crawford, W. C., R. A. Stephen, and S. T. Bolmer (2006). A second look at low-frequency marine vertical seismometer data quality at the OSN-1 site off Hawaii for seafloor, buried, and borehole emplacements, *Bull. Seismol. Soc. Am.* **96,** no. 5, 1952–1960.

Dahm, T., F. Tilmann, and J. P. Morgan (2006). Seismic broadband ocean-bottom data and noise observed with free-fall stations: Experiences from long-term deployments in the North Atlantic and the Tyrrhenian sea, *Bull. Seismol. Soc. Am.* **96,** no. 2, 647–664.

Duennebier, F., and G. Sutton (1995). Fidelity of ocean bottom seismic observations, *Mar. Geophys. Res.* **17,** no. 6, 535–555.

Duennebier, F. K., G. Blackinton, and G. H. Sutton (1981). Current-generated noise recorded on ocean bottom seismometers, *Mar. Geophys. Res.* **5,** no. 1, 109–115.

Graizer, V. (2006). Tilts in strong ground motion, *Bull. Seismol. Soc. Am.* **96,** no. 6, 2090–2102.

Graizer, V. (2009). The response to complex ground motions of seismometers with Galperin sensor configuration, *Bull. Seismol. Soc. Am.* **99,** no. 2B, 1366–1377.

Hadziioannou, C., P. Gaebler, U. Schreiber, J. Wassermann, and H. Igel (2012). Examining ambient noise using colocated measurements of rotational and translational motion, *J. Seismol.* **16,** no. 4, 787–796.

Hunter, J. D. (2007). Matplotlib: A 2D graphics environment, *Comput. Sci. Eng.* **9,** no. 3, 90–95.

Igel, H., U. Schreiber, A. Flaws, B. Schuberth, A. Velikoseltsev, and A. Cochard (2005). Rotational motions induced by the *M* 8.1 Tokachi-oki earthquake, September 25, 2003, *Geophys. Res. Lett.* **32,** no. 8, L08309.

Kedar, S., M. Longuet-Higgins, F. Webb, N. Graham, R. Clayton, and C. Jones (2008). The origin of deep ocean microseisms in the North Atlantic Ocean, *Proc. Math. Phys. Sci.* **464,** 777–793.

Longuet-Higgins, M. S. (1950). A theory of the origin of microseisms, *Philos. Trans. Math. Phys. Sci.* **243,** no. 857, 1–35.

McLeod, D. P., G. E. Stedman, T. H. Webb, and U. Schreiber (1998). Comparison of standard and ring laser rotational seismograms, *Bull. Seismol. Soc. Am.* **88,** no. 6, 1495–1503.

Megies, T., M. Beyreuther, R. Barsch, L. Krischer, and J. Wassermann (2011). Obspy—What can it do for data centers and observatories? *Ann. Geophys.* **54,** no. 1, 47–58.

Pancha, A., T. H. Webb, G. E. Stedman, D. P. McLeod, and K. U. Schreiber (2000). Ring laser detection of rotations from teleseismic waves, *Geophys. Res. Lett.* **27,** no. 21, 3553–3556.

Peterson, J. (1993). Observations and modeling of seismic background noise, *U.S. Geol. Surv. Open-File Rept. 93-322.*

Pillet, R., A. Deschamps, D. Legrand, J. Virieux, N. Béthoux, and B. Yates (2009). Interpretation of broadband ocean-bottom seismometer horizontal data seismic background noise, *Bull. Seismol. Soc. Am.* **99,** no. 2B, 1333–1342.

Rodgers, P. (1968). The response of the horizontal pendulum seismometer to Rayleigh and love waves, tilt, and free oscillations of the earth, *Bull. Seismol. Soc. Am.* **58,** no. 5, 1385–1406.

Schreiber, K. U., A. Velikoseltsev, A. J. Carr, and R. Franco-Anaya (2009). The application of fiber optic gyroscopes for the measurement of rotations in structural engineering, *Bull. Seismol. Soc. Am.* **99,** no. 2B, 1207–1214.

Stähler, S. C., K. Sigloch, K. Hosseini, W. C. Crawford, G. Barruol, M. C. Schmidt-Aursch, M. Tsekhmistrenko, J.-R. Scholz, A. Mazzullo, and M. Deen (2016). Performance report of the RHUM-RUM ocean bottom seismometer network around La Réunion, western Indian Ocean, *Adv. Geosci.* **41,** 43–63.

Sutton, G., W. McDonald, D. Prentiss, and S. Thanos (1965). Ocean-bottom seismic observatories, *Proc. IEEE* **53,** no. 12, 1909–1921.

Tolman, H. L. (1997). A new global wave forecast system at NCEP, *Ocean Wave Meas. Anal.* **2,** 777–786.

Tolman, H. L. (2009). User manual and system documentation of WAVEWATCH III TM version 3.14, *Technical note, MMAB Contribution, 276*.

Webb, S. (1988). Long-period acoustic and seismic measurements and ocean floor currents, *IEEE J. Ocean. Eng.* **13,** no. 4, 263–270.

Webb, S. C. (1998). Broadband seismology and noise under the ocean, *Rev. Geophys.* **36,** no. 1, 105–142.

Webb, S. C., and W. C. Crawford (2010). Shallow-water broadband OBS seismology, *Bull. Seismol. Soc. Am.* **100,** no. 4, 1770–1778.

Yang, Z., A. F. Sheehan, J. A. Collins, and G. Laske (2012). The character of seafloor ambient noise recorded offshore New Zealand: Results from the Moana Ocean bottom seismic experiment, *Geochem. Geophys. Geosys.* **13,** no. 10, Q10011.

***Fabian Lindner*[1]**
Joachim Wassermann
Heiner Igel
Department of Earth and Environmental Sciences
Ludwig-Maximilians-University of Munich
Theresienstraße 41
80333 Munich
Germany

Mechita C. Schmidt-Aursch
Alfred Wegener Institute
Helmholtz Centre for Polar and Marine Research
Am Alten Hafen 26
27568 Bremerhaven
Germany

Karl Ulrich Schreiber
Forschungseinrichtung Satellitengeodäsie
Technical University of Munich
Fundamentalstation Wettzell, Sackenrieder Straße 25
93444 Bad Kötzting
Germany

Published Online 2 November 2016

[1] Now at the Laboratory of Hydraulics, Hydrology and Glaciology (VAW), ETH Zürich, Hönggerbergring 26, 8093 Zürich, Switzerland; ***lindner@vaw.baug.ethz.ch.***